Arabian Journal for Science and Engineering (2019) 44:739–752
https://doi.org/10.1007/s13369-018-3260-9

RESEARCH ARTICLE - MECHANICAL ENGINEERING

Analytical Solution for Fully Developed Flows of Nanofluids in Mixed-Convection Zone Within Vertical Channels

Fahad G. Al-Amri[1]

Received: 3 October 2017 / Accepted: 12 April 2018 / Published online: 23 April 2018

Abstract

In this paper, a closed-form analytical solution is presented for a fully developed mixed-convection laminar flow of nanofluids between two vertical parallel plates. The Buongiorno model, which considers the Brownian motion and thermophoresis force, is employed to investigate the hydrodynamic and heat transfer behavior of the nanofluid flow. The equations for the conservation of mass, momentum, energy, and the nanoparticle concentration field have been analytically solved, and expressions for the velocity, temperature, and nanoparticle concentration profiles as well as for the Nusselt number are given. The results show that in addition to the mixed-convection buoyancy parameter (Gr/Re), the immersed-particle buoyancy parameter additionally enriches the momentum and enhances the heat transfer inside the channel. Moreover, in the mixed-convection regime, in contrast to the case of forced convection, the heat transfer rate decreases sharply and then gradually as the solid/fluid thermal conductivity ratio increases. The present results contradict the prevailing perception that higher thermal conductivities of nanoparticles are always desirable and boost heat transfer. The study findings will be helpful in selecting an appropriate nanoparticle material that would provide a high heat transfer rate based on the application's thermal conditions.

Keywords Nanofluid · Vertical plate · Mixed convection · Brownian motion · Thermophoresis

List of symbols

b	Channel spacing
C_p	Specific heat at constant pressure
d_p	Nanoparticle diameter
D_B	Brownian diffusivity, $= K_\mathrm{BO}T/3\pi\mu_\mathrm{bf}d_\mathrm{p}$
D_T	Thermophoresis diffusivity, $= 0.26k_\mathrm{bf}/(2k_\mathrm{bf}+k_\mathrm{p})*\mu_\mathrm{bf}/\rho_\mathrm{bf}*\phi_0$
Gr	Grashof number, $\frac{g\beta_\mathrm{bf}q_1b^4}{\upsilon^2K_\mathrm{bf}}$
K	Thermal conductivity
K_BO	Boltzmann constant
Kr	Solid/fluid thermal conductivity ratio, $K_\mathrm{p}/K_\mathrm{bf}$
N_BT	Ratio of Brownian and thermophoretic diffusivities, $= D_\mathrm{B}/D_\mathrm{T}$
Nu	Nusselt number
p	Fluid pressure at any cross section
p'	Pressure defect at any cross section, $p-p_\mathrm{s}$
p_0	Fluid pressure at channel entrance
p_s	Hydrostatic pressure, $-\rho_0\,gz$
P	Dimensionless pressure at any cross section, $\frac{p'-p_0}{\rho_0u_0^2}$
Pr	Prandtl number
r_q	Heat flux ratio, $\frac{q_2}{q_1}$
Re	Reynolds number, $= \frac{u_\mathrm{o}b}{\upsilon}$
T	Temperature at any point
T_0	Inlet temperature
T_m	Mean temperature in each cross section $T_\mathrm{m}(z)$
u_o	Entrance axial velocity
u	Longitudinal velocity component at any point
U	Dimensionless longitudinal velocity, $= u/u_\mathrm{o}$
y	Horizontal coordinate
Y	Dimensionless horizontal coordinate, y/b
z	Vertical coordinate
Z	Dimensionless vertical coordinate, $z/(bRe)$

Greek symbols

υ	Kinematic fluid viscosity
ρ	Fluid density
μ	Dynamic fluid viscosity

✉ Fahad G. Al-Amri
fgalamri@iau.edu.sa

[1] Department of Mechanical and Energy Engineering, College of Engineering, Imam Abdulrahman Bin Faisal University, P.O. Box 1982, Dammam 31441, Saudi Arabia

θ	Dimensionless temperature at any point, $[= \frac{k_{\mathrm{bf}}(T-T_{\mathrm{m}})}{q_1 b}]$
β	Thermal expansion coefficient
ϕ	Particle volume fraction
Φ	Rescaled nanoparticle volume fraction, $[= \frac{\phi}{\phi_0}]$
γ	Immersed-particle buoyancy parameter, $= 0.78\pi \frac{\mu_{\mathrm{bf}}^2}{\rho_{\mathrm{bf}}} \frac{\mathrm{d_p}}{K_{\mathrm{BO}}\beta_{\mathrm{bf}} T_0^2} (\frac{\rho_{\mathrm{p}}}{\rho_{\mathrm{bf}}} - 1)$

Subscripts

bf	Base fluid
nf	Nanofluid
m	Mean
w	Wall
p	Particle
1	Duct wall at $Y = 0$
2	Duct wall at $Y = 1$
0	Condition at the entrance

1 Introduction

Thermal conductivity of the classic heat transfer fluids such as oil and water is low, which restricts the use of these fluids as a coolant medium in several engineering applications that require the dissipation of high heat flux. The need to develop high-thermal-conductivity coolants capable of dissipating the high heat flux encountered in such applications, and the advances in modern nanotechnology have led to the development of the innovative technique of suspending nanoscale particles in a fluid to form a dilute mixture called a "nanofluid" [1]. Nanoparticles have been found to possess several advantages over milliparticles and microparticles: they produce long-term stable nanofluids [2], have higher surface-area-to-volume ratios, exhibit useful random movement [3], can act as lubricating medium [4], have less particle clogging [5], and have abnormally high thermal conductivity at quite low particle concentration [6]. The development of an appropriate model for the convective transport of nanofluids is the key to utilizing a particular nanofluid for heat transfer applications. Three main models are used to theoretically evaluate the heat transfer enhancement due to the addition of low-concentration nanoparticles to conventional working fluids: homogeneous (single-phase), dispersion, and nonhomogeneous models. In the homogeneous model, the nanofluid is treated as a conventional fluid with a modified transport coefficient to take into account the effect of solid particles dispersed in the base fluid [7]. The unique transport properties of nanofluids compared to pure fluids result in heat transfer enhancement; however, several experimental studies [8,9] have shown that the increase in the heat transfer coefficient remarkably exceeds the supposed increment because of the enhancement in the thermophysical properties of the nanofluid. In the thermal dispersion model [10], anomalous heat transfer enhancement is attributed to the irregular movements of nanoparticles; these movements are treated as perturbations in the energy equation. The nonhomogeneous model takes into account the relative velocity between nanoparticles and the base fluid [11]. Buongiorno [12] analyzed seven slip mechanisms that can generate a relative velocity between a nanosolid and the base fluid and found that only Brownian diffusion and thermophoresis are influential mechanisms in nanofluids. He developed a two-component four-equation nonhomogeneous equilibrium model for convection transport in nanofluids.

These three models have been extensively used to investigate the problem of fully developed convection heat transfer in nanofluids inside channels. Chen et al. [13] numerically investigated the heat transfer performance of a mixed-convection nanofluid flow in a vertical channel with an isothermal boundary condition. They employed the homogeneous model and observed a reduction in the average entropy generation of the nanofluid compared to that of pure water. Heris et al. [14] used the dispersion model to numerically investigate the laminar convective heat transfer enhancement of nanofluids inside a tube. They found that the heat transfer coefficient decreases with the nanoparticle size at a particular concentration. The homogeneous model was employed to obtain an analytical solution for the opposing mixed-convection flow in an inclined channel [15]. It was found that the volume fraction delays the occurrence of flow reversal. The same model was used to study fully developed buoyancy-assisted and buoyancy-opposed flows in a vertical channel filled with nanofluids [16]. The nanoparticle volume fraction was found to enhance the heat and mass transfer characteristics of the fluids. The nonhomogeneous Buongiorno model was used to obtain closed-form analytical solutions of laminar mixed convection between two vertical plates with isothermal boundary conditions [17]. It was shown that Brownian motion and thermophoresis have a significant effect on the shape of the velocity and temperature profiles. The same model was used to study the steady laminar forced convection between two plates involving nanofluids with periodic and linearly varying boundary conditions [18]. In the case of periodic boundary conditions, it was found that migration has an obvious effect on the solution; however, in the case of a longitudinally linearly varying boundary temperatures, the volumetric concentration of nanoparticles was found to be a weak function of the temperature profile.

The previous studies reveal that nanoparticle migration has noticeable effects on the thermal performance of nanofluids [17,18]. Until now, a few investigators have studied the effect of the migration phenomenon in the mixed-convection

channel flow with isothermal boundary conditions. In these studies, the distribution of the nanoparticles at the boundary is assumed to be constant, which could be practically unrealistic. The problem is still not well understood, and the interaction of Brownian motion and thermophoresis with buoyancy force needs further investigation. Moreover, to the best of the author's knowledge, the problem of a fully developed mixed-convection flow of nanofluids between two vertical parallel plates with isoflux boundary conditions while considering nanoparticle migration has not yet been solved. The present work is motivated by the importance of this problem in many engineering applications such as electronic device cooling, heat exchanger operations, nuclear system operations, and thermal waste heat management of new power weapons [19,20]. Therefore, the present study aims to analytically solve this problem using the Buongiorno model. The nanoparticle distribution at the boundary is determined as part of the solution using the nanoparticle conservation equation and applying "the no mass flux of solid particle condition" at the walls. The effects of the mixed-convection buoyancy parameter, immersed-particle buoyancy parameter, volume fraction, thermal conductivity ratio, and heat flux ratio on the solution are investigated.

2 Mathematical Formulation and Solution

2.1 Problem Description and Thermophysical Properties

In the present study, a fully developed mixed-convection flow of a water-based nanofluid between two vertical parallel plates is considered where asymmetric heating is imposed on the two surfaces of the channel formed by the plates. The flow is assumed to be steady and laminar with uniform velocity (u_0), temperature (T_0), and volume fraction (ϕ_0) distributions at the channel entrance [21]. The nanoparticles and base fluid are assumed to form a dilute mixture and to be in thermal equilibrium. These two assumptions have been theoretically proven to be justified by Buongiorno [12]. Furthermore, for ($\phi_0 < 1\%$), nanofluids appear macroscopically as homogeneous fluids and their transport properties can be accurately determined based on the physical principle of the mixture rule. Escher et al. [22] experimentally found that the thermophysical properties of nanofluids deviate less than 10% from the general rule of mixtures even at a high volume fraction (up to 3%). The schematic geometry of the problem is shown in Fig. 1, and the thermophysical properties of the base fluid and nanoparticles used in the present work are listed in Table 1. The viscosity, density, heat capacity at a constant pressure, and thermal conductivity of the nanofluid are defined as follows [23]:

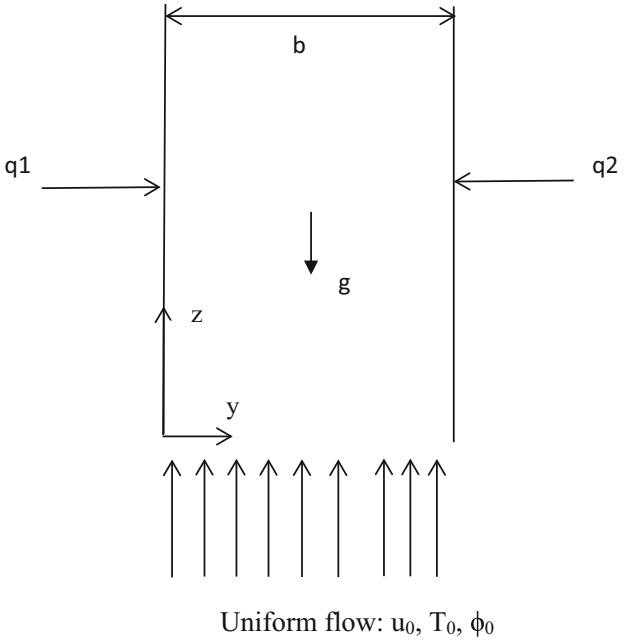

Fig. 1 Schematic geometry of problem and coordinate system

Table 1 Thermophysical properties of base fluid and nanoparticles [24–26]

Properties	Water	Cu	Al_2O_3	SiO_2
ρ (kg/m^3)	997	8933	3920	2200
K (W/m k)	0.613	400	36	1.38
μ (kg/m s)	0.000866	–	–	–

$$\mu_{\mathrm{nf}} = \frac{\mu_{\mathrm{bf}}}{(1-\phi_{\mathrm{o}})^{2.5}}$$

$$\rho_{\mathrm{nf}} = (1-\phi_{\mathrm{o}})\,\rho_{\mathrm{bf}} + \phi_{\mathrm{o}}\rho_{\mathrm{p}}$$

$$C_{p_{\mathrm{nf}}} = \frac{\phi_0\rho_{\mathrm{p}}C_{p_{\mathrm{p}}} + (1-\phi_0)\rho_{\mathrm{bf}}C_{\mathrm{bf}}}{\rho_{\mathrm{nf}}}$$

$$K_{\mathrm{nf}} = K_{\mathrm{bf}}\left[\frac{K_{\mathrm{p}} + 2K_{\mathrm{bf}} - 2\phi_0\left(K_{\mathrm{bf}} - K_{\mathrm{p}}\right)}{K_{\mathrm{p}} + 2K_{\mathrm{bf}} + \phi_{\mathrm{o}}\left(K_{\mathrm{bf}} - K_{\mathrm{p}}\right)}\right]$$

2.2 Nanoparticle Migration

Two main nanoparticle migration mechanisms are significant in nanofluids: Brownian and thermophoretic diffusivities [12]. In Brownian motion, the continuous collisions between solid particles and liquid molecules lead to random swimming of suspended particles in the base fluid. Thus, the Brownian diffusion is proportional to the concentration gradient and causes a nanoparticle mass flux that can be obtained from the following relationship:

$$j_{\mathrm{p,B}} = -\rho_{\mathrm{p}} D_{\mathrm{B}} \nabla\phi \tag{1}$$

Here, D_{B} is the Brownian diffusion coefficient given by the Einstein–Stokes equation:

$$D_{\mathrm{B}} = \frac{k_{\mathrm{B}} T}{3\pi \mu_{\mathrm{bf}} d_{\mathrm{p}}}$$

On the other hand, thermophoresis causes nanoparticle migration from warmer to colder regions (i.e., in the direction opposite to the temperature gradient). The nanoparticle flux due to thermophoresis can be given as follows:

$$j_{\mathrm{p,T}} = -\rho_{\mathrm{p}} D_{\mathrm{T}} \frac{\nabla T}{T} \tag{2}$$

Here, D_{T} is the thermal diffusion given by

$$D_{\mathrm{T}} = 0.26 \frac{k_{\mathrm{bf}}}{2k_{\mathrm{bf}} + k_{\mathrm{p}}} \frac{\mu_{\mathrm{bf}}}{\rho_{\mathrm{bf}}} \phi$$

Therefore, the continuity equation for the nanoparticles can be written in the following form:

$$D_{\mathrm{B}} \frac{\mathrm{d}^2 \phi}{\mathrm{d}y^2} + \frac{D_{\mathrm{T}}}{T_{\mathrm{m}}} \frac{\mathrm{d}^2 T}{\mathrm{d}y^2} = 0 \tag{3}$$

2.3 Governing Equations

In the absence of a chemical reaction, radiation transfer, and viscous dissipation and by employing the Oberbeck–Boussinesq approximation, the equations for the conservation of momentum and energy in the fully developed region can be written as follows [17]:

$$-\frac{\mathrm{d}P}{\mathrm{d}z} + \mu_{\mathrm{nf}} \frac{\mathrm{d}^2 u}{\mathrm{d}y^2} + [(1-\phi_0)\rho_{\mathrm{bf}_0}\beta_{\mathrm{bf}}(T - T_{\mathrm{m}}) - (\rho_{\mathrm{p}} - \rho_{\mathrm{bf}})(\phi - \phi_0)]g = 0 \tag{4}$$

$$(\rho C_{\mathrm{P}})_{\mathrm{nf}} u \frac{\mathrm{d}T}{\mathrm{d}z} = k_{\mathrm{nf}} \frac{\mathrm{d}^2 T}{\mathrm{d}y^2} \tag{5}$$

It is worth mentioning that the mean fluid temperature in each cross section $T_{\mathrm{m}}(z)$ has been selected as a reference fluid temperature, as proposed by Barletta and Zanchini [27].

The above momentum and energy equations in addition to the nanoparticle concentration equation [Eq. (3)] embody the problem under consideration, and these three equations can be written in dimensionless forms as follows:

$$\frac{\mathrm{d}^2 U}{\mathrm{d}Y^2} - (1-\phi_0)^{2.5} \frac{\mathrm{d}P}{\mathrm{d}Z} + \frac{Gr}{Re}\left[(1-\phi_0)^{3.5}\theta - \frac{\gamma}{2+\mathrm{Kr}}\phi_0 (1-\phi_0)^{2.5} N_{\mathrm{BT}} (\Phi - 1)\right] = 0 \tag{6}$$

$$Pr\left[\phi_0 \frac{(\rho C_{\mathrm{p}})_{\mathrm{p}}}{(\rho C_{\mathrm{p}})_{\mathrm{bf}}} + (1-\phi_0)\right] U \frac{\partial \theta}{\partial Z} = \left[\frac{\mathrm{Kr} + 2 - 2\phi_0 (1 - \mathrm{Kr})}{\mathrm{Kr} + 2 + \phi_0 (1 - \mathrm{Kr})}\right] \frac{\partial^2 \theta}{\partial Y^2} \tag{7}$$

$$N_{\mathrm{BT}} \frac{\partial^2 \Phi}{\partial Y^2} + \frac{\partial^2 \theta}{\partial Y^2} = 0 \tag{8}$$

The definitions of the nondimensional quantities in the above equations are found in List of symbols.

The pressure gradient in the momentum equation can be determined by employing the mass flux concentration of the nanoparticles.

$$\int_0^1 \Phi \, \mathrm{d}y = 0 \tag{9}$$

2.4 Boundary Conditions

The boundary conditions are

$$U(0) = 0 \quad \text{and} \quad U(1) = 0 \tag{10}$$

$$\frac{\partial \theta}{\partial Y}|_{y=0} = -\frac{K_{\mathrm{bf}}}{K_{\mathrm{nf}}} \text{ and } \frac{\partial \theta}{\partial Y}|_{y=1} = \frac{K_{\mathrm{bf}}}{K_{\mathrm{nf}}} r_{\mathrm{q}} \tag{11}$$

Moreover, because the wall is impermeable, one can write [28]

$$N_{\mathrm{BT}} \frac{\partial \theta}{\partial Y}|_{Y=0} + \frac{\partial \theta}{\partial Y}|_{Y=0} = 0 \text{ at } Y = 0 \text{ and } N_{\mathrm{BT}} \frac{\partial \theta}{\partial Y}|_{Y=1} + \frac{\partial \theta}{\partial Y}|_{Y=1} = 0 \text{ at } Y = 1 \tag{12}$$

At the channel entrance, the boundary conditions are

$$U = 1, \theta = 1 \text{ and } \Phi = 1 \text{ at } Z = 0 \tag{13}$$

The dimensionless parameters used in the above boundary conditions are defined in the List of symbols section.

2.5 Analytical Solution

By integrating Eq. (8) twice and applying the boundary conditions [Eqs. (12) and (13)], one can find a solution for the particle concentration as a function of the temperature distribution inside the channel as

$$\Phi = -\frac{1}{N_{\mathrm{BT}}}\theta + 1 \tag{14}$$

By considering an energy balance inside the channel for a thermally fully developed flow, the first gradient of the temperature can be written as

$$\frac{\partial \theta}{\partial Z} == \frac{1 + r_{\mathrm{q}}}{Pr_{+} Pr \phi_{\mathrm{o}} \left[\frac{(\rho c_{\mathrm{p}})_{\mathrm{p}}}{(\rho c_{\mathrm{p}})_{\mathrm{bf}}} - 1\right]} \tag{15}$$

Thus, the energy equation can be written as

$$U = \beta \frac{\partial^2 \theta}{\partial Y^2} \tag{16}$$

where

$$\beta = \frac{K_{\mathrm{p}} + 2K_{\mathrm{bf}} - 2\phi_{\mathrm{o}}\left(K_{\mathrm{bf}} - K_{\mathrm{p}}\right)}{K_{\mathrm{p}} + 2K_{\mathrm{bf}} + \phi_{\mathrm{o}}\left(K_{\mathrm{bf}} - K_{\mathrm{p}}\right)\left(1 + r_{\mathrm{q}}\right)}$$

Substituting Eq. (14) into the momentum equation [Eq. (6)] gives

$$\frac{\mathrm{d}^2 U}{\mathrm{d}Y^2} - (1-\phi_{\mathrm{o}})^{2.5}\frac{\mathrm{d}P}{\mathrm{d}Z} + \frac{Gr}{Re}\left[(1-\phi_{\mathrm{o}})^{3.5} + \frac{\gamma}{(2+\mathrm{Kr})}\phi_{\mathrm{o}}\,(1-\phi_{\mathrm{o}})^{2.5}\right]\theta = 0 \tag{17}$$

Rearranging Eq. (17) gives

$$\theta = \left[-\frac{\mathrm{d}^2 U}{\mathrm{d}Y^2} + (1-\phi_{\mathrm{o}})^{2.5}\frac{\mathrm{d}P}{\mathrm{d}Z}\right] \Big/ \left\{\frac{Gr}{Re}\left[(1-\phi_{\mathrm{o}})^{3.5} + \frac{\gamma}{(2+\mathrm{Kr})}\phi_{\mathrm{o}}\,(1-\phi_{\mathrm{o}})^{2.5}\right]\right\} \tag{18}$$

Taking the second derivative of the above equation on Y gives the following equation:

$$\frac{\partial^2 \theta}{\partial Y^2} = -\frac{\mathrm{d}^4 U}{\mathrm{d}Y^4} \Big/ \left\{\frac{Gr}{Re}\left[(1-\phi_{\mathrm{o}})^{3.5} + \frac{\gamma}{(2+\mathrm{Kr})}\phi_{\mathrm{o}}\,(1-\phi_{\mathrm{o}})^{2.5}\right]\right\} \tag{19}$$

Substituting Eq. (19) into Eq. (16) yields

$$U = -a^4 \frac{\mathrm{d}^4 U}{\mathrm{d}Y^4} \tag{20}$$

where $a = \left[\frac{\beta}{\frac{Gr}{Re}\left[(1-\phi_{\mathrm{o}})^{3.5} + \frac{\gamma}{(2+\mathrm{Kr})}\phi_{\mathrm{o}}(1-\phi_{\mathrm{o}})^{2.5}\right]}\right]^{0.25}$

The exact solution of the above equation can be written in the following form:

$$U(Y) = C_1 \exp(aY)\cos(aY) + C_2 \exp(-aY)\cos(aY) + C_3 \exp(aY)\sin(aY) + C_4 \exp(-aY)\sin(aY)$$

By applying the four boundary conditions given in Eqs. (10) and (11), the four unknown constants can be obtained as

$$C_1 = \frac{\sin(a)\left[b_1 \sin(a) - b_2 \sinh(a)\right]}{2a^3\left[-2 + \cos(2a) + \cosh(2a)\right]} = -C_2$$

$$C_3 = -\left\{-2b_2 e^{-\mathrm{a}}\sin(a) + b_1\left(1 - e^{-2\mathrm{a}} + \sin(2a)\right) - 2b_2\cos(a)\sinh(a)\right\}$$

$$C_4 = e^{-\mathrm{a}}\left\{b_1 e^{3\mathrm{a}} + b_2\cos(a) - b_2 e^{2\mathrm{a}}\left[\cos(a) + 2\sin(a)\right] + b_1 e^{\mathrm{a}}\left[-1 + \sin(2a)\right]\right\} \Big/ \left\{4a^3\left(-2 + \cos(2a) + cosh(2a)\right)\right\}$$

where

$$b_1 = \frac{K_{\mathrm{bf}}}{K_{\mathrm{nf}}}\left\{\frac{Gr}{Re}\left[(1-\phi_{\mathrm{o}})^{3.5} + \frac{\gamma}{(2+\mathrm{Kr})}\phi_{\mathrm{o}}\,(1-\phi_{\mathrm{o}})^{2.5}\right]\right\}$$

$$b_2 = -\frac{K_{\mathrm{bf}}}{K_{\mathrm{nf}}} r_{\mathrm{q}}\left\{\frac{Gr}{Re}\left[(1-\phi_{\mathrm{o}})^{3.5} + \frac{\gamma}{(2+\mathrm{Kr})}\phi_{\mathrm{o}}\,(1-\phi_{\mathrm{o}})^{2.5}\right]\right\}$$

By using Eq. (14), one can write Eq. (9) in the following form:

$$\int_0^1 \theta \,\mathrm{d}Y = 0 \tag{21}$$

The above equation is consistent with the definition of θ, and from Eq. (18), the pressure gradient can be expressed in the following form:

$$\frac{\mathrm{d}P}{\mathrm{d}Z} = \left[\frac{\mathrm{d}U}{\mathrm{d}Y}|_{Y=1} - \frac{\mathrm{d}U}{\mathrm{d}Y}|_{Y=0}\right] \Big/ (1-\phi_{\mathrm{o}})^{2.5}$$

Further, one can write the pressure gradient in the following form:

$$\frac{\mathrm{d}P}{\mathrm{d}Z} = \frac{(b_1 - b_2)\left\{\sin(a) + \sinh(a)\right\}}{2a^2\,(1-\phi_{\mathrm{o}})^{2.5}\left\{\sin(a) - \sinh(a)\right\}} \tag{22}$$

Now, Eq. (18) can be used to derive the following form for the dimensionless temperature:

$$\theta = \left[-\left\{2a^2\cos(aY)\left(C_3 e^{\mathrm{aY}} - C_4 e^{-\mathrm{aY}}\right) + 2a^2 C_2 \sin(aY)\left(e^{-\mathrm{aY}} + e^{\mathrm{aY}}\right)\right\} + (1-\phi_{\mathrm{o}})^{2.5}\frac{\mathrm{d}P}{\mathrm{d}Z}\right] \Big/ \left\{\frac{Gr}{Re}\left[(1-\phi_{\mathrm{o}})^{3.5} + \frac{\gamma}{(2+\mathrm{Kr})}\phi_{\mathrm{o}}\,(1-\phi_{\mathrm{o}})^{2.5}\right]\right\} \tag{23}$$

The local Nusselt number on the first wall is defined in the present study as

$$Nu = \frac{-b\frac{\partial T}{\partial y}|_{y=0}}{T_{\mathrm{w}} - T_{\mathrm{m}}}\frac{K_{\mathrm{nf}}}{K_{\mathrm{bf}}} = -\mathrm{Kr}\frac{\frac{\partial \theta}{\partial Y}|_{Y=0}}{\theta_{\mathrm{w}}}$$

Hence, the following form is deduced for the Nusselt number:

Table 2 Comparison between the present results and the correlation of Xuan and Roetzel [29] for heat transfer enhancement for forced-convection laminar flow ($Gr/Re = 0.001$, $\gamma = 112{,}000$, $r_q = 1$)

Φ_0	Cu			SiO_2		
	h_{nf}/h_{bf} (Xuan and Roetzel [29])	h_{nf}/h_{bf} (present work)	Deviation %	h_{nf}/h_{bf} (Xuan and Roetzel [29])	h_{nf}/h_{bf} (present work)	Deviation %
0.002	1.018060894	1.018062262	0.000134415	1.005310267	1.005447457	0.013646535
0.004	1.036411452	1.036414159	0.000261153	1.010645592	1.010918023	0.026956196
0.006	1.055056034	1.055058872	0.000268985	1.016006086	1.01641579	0.040324985
0.008	1.073999065	1.074003706	0.000432124	1.021391861	1.02193682	0.053354549
0.01	1.093245039	1.093249908	0.000445358	1.026803028	1.0274832	0.066241638

Uniform flow: u_0, T_0, ϕ_0

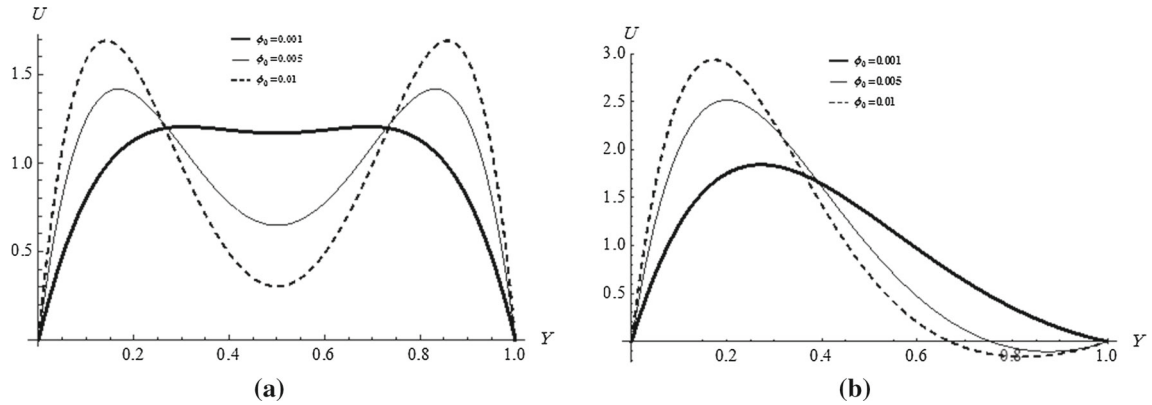

Fig. 2 Dimensionless velocity distribution of nanofluid for different values of ϕ_0 ($Gr/Re = 100$, $\gamma = 1{,}120{,}000$, Kr = 652): **a** $r_q = 1$ and **b** $r_q = 0$

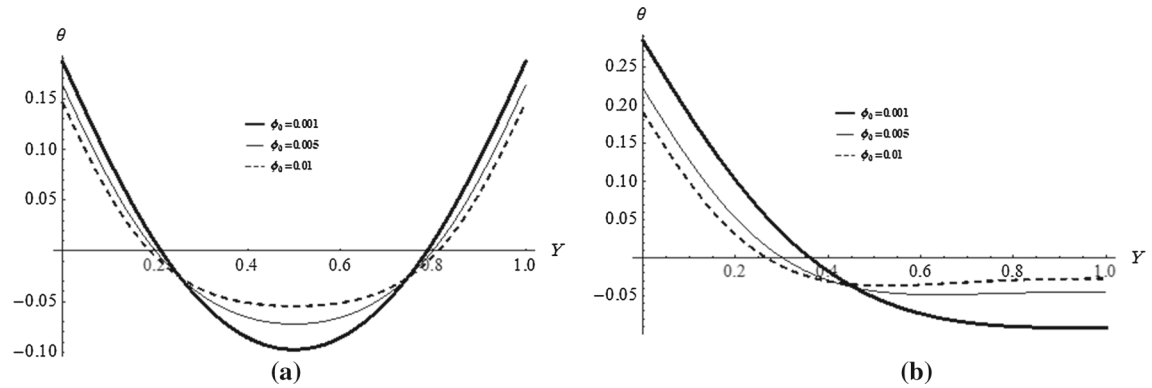

Fig. 3 Dimensionless temperature distribution of nanofluid for different values of ϕ_0 ($Gr/Re = 100$, $\gamma = 1{,}120{,}000$, Kr = 652): **a** $r_q = 1$ and **b** $r_q = 0$

$$Nu = \left\{2a^2 b_1 \left(-2 + \cos(2a) + \cosh(2a)\right)\right\} / \left\{\begin{pmatrix} (b_1 - b_2)\cos(2a) + (-b_1 + b_2)\cosh(2a) - 4ab_2\cosh(a)\sin(a) + 2ab_1\sin(2a) + \\ 4\left(-ab_2\cos(a) + ab_1\cosh(a) + (-b_1 + b_2)\sin(a)\right)\sinh(a) \end{pmatrix}\right\} \tag{24}$$

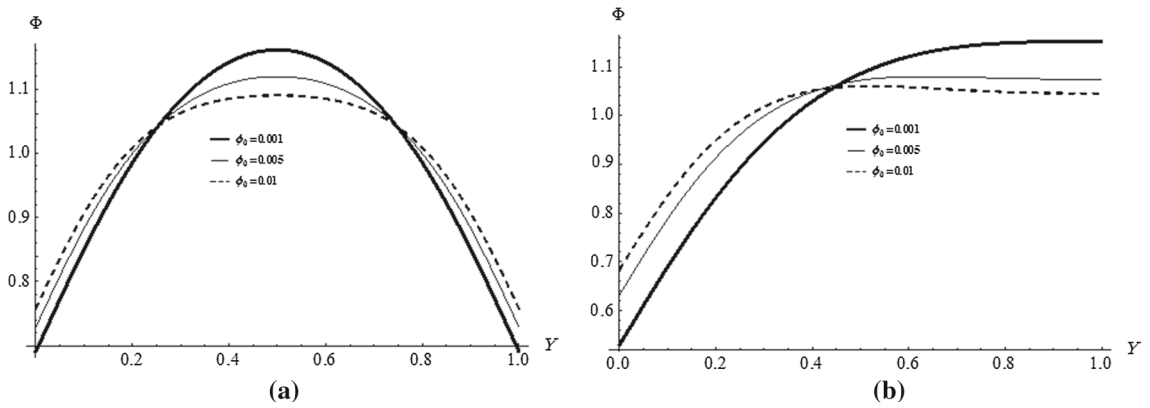

Fig. 4 Dimensionless nanoparticle distribution for different values of ϕ_0 ($Gr/Re = 100$, $\gamma = 1{,}120{,}000$, Kr = 652): **a** $r_q = 1$ and **b** $r_q = 0$

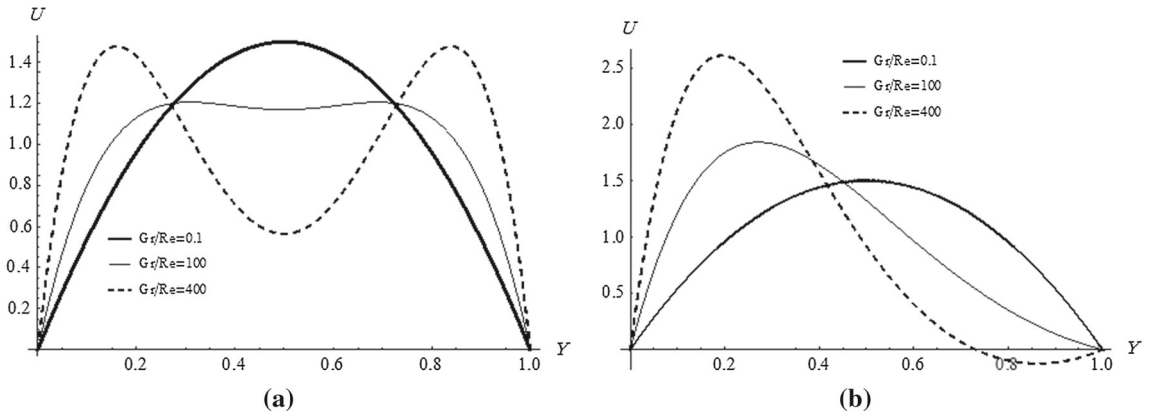

Fig. 5 Dimensionless velocity distribution of nanofluid for different values of Gr/Re ($\phi_0 = 0.001$, $\gamma = 1{,}120{,}000$, Kr = 652): **a** $r_q = 1$ and **b** $r_q = 0$

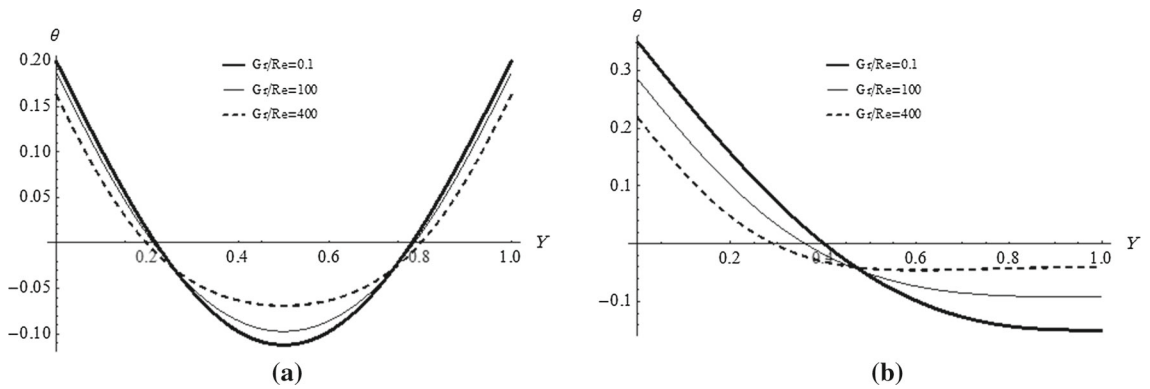

Fig. 6 Dimensionless temperature distribution of nanofluid for different values of Gr/Re ($\phi_0 = 0.001$, $\gamma = 1{,}120{,}000$, Kr = 652): **a** $r_q = 1$ and **b** $r_q = 0$

Note that the present approach and the solution are limited to tiny nanoparticles ($d_p < 100$ nm) and to dilute suspensions ($\phi < 1\%$).

2.6 Validation

In the forced-convection regime, the heat transfer enhancement is mainly due to the increase in the effective thermal conductivity of the nanofluids. Xuan and Roetzel [29] obtained the following correlation for heat transfer enhancement for laminar flow:

$$\frac{h_{nf}}{h_{bf}} \approx \left(\frac{k_{nf}}{k_{bf}}\right)^3 \tag{25}$$

To validate the present results, the heat transfer enhancement when $Gr/Re \approx 0$ (i.e., pure forced convection) is calculated

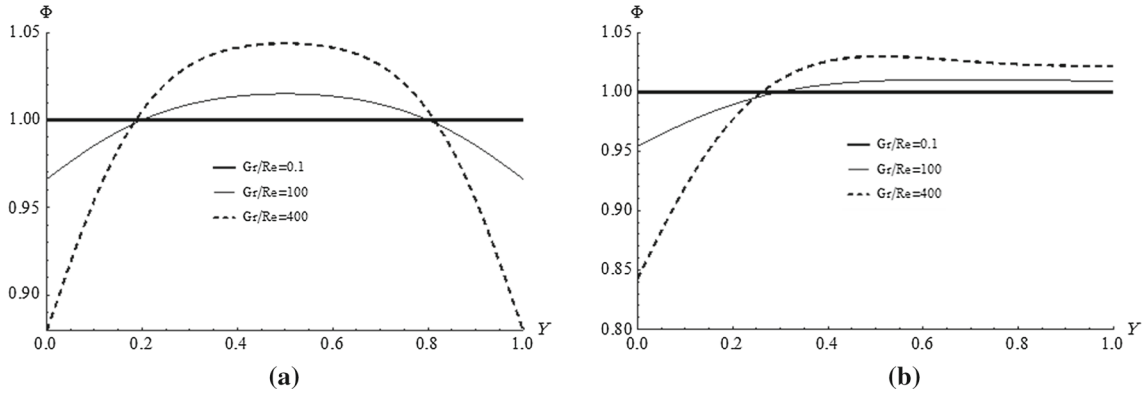

Fig. 7 Dimensionless particle distribution of nanofluid for different values of Gr/Re ($\phi_0 = 0.001$, $\gamma = 1{,}120{,}000$, Kr = 652): **a** $r_q = 1$ and **b** $r_q = 0$

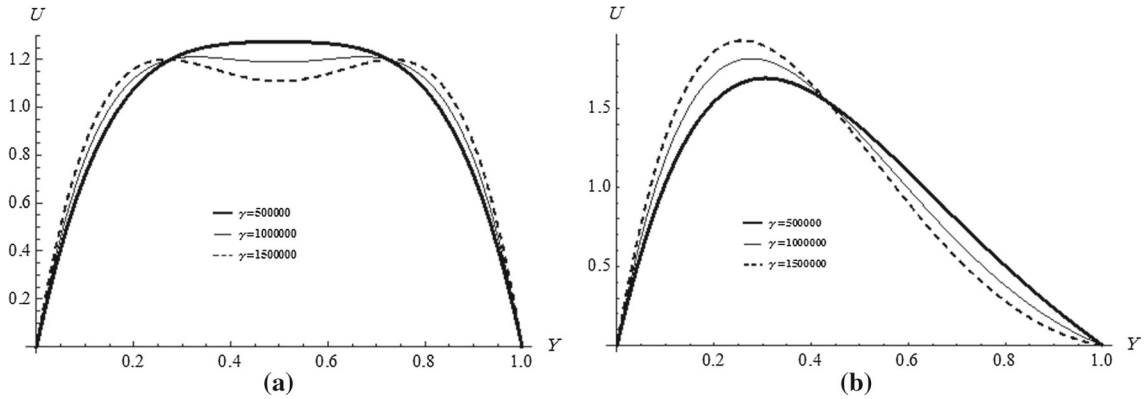

Fig. 8 Dimensionless velocity distribution of nanofluid for different values of γ ($\phi_0 = 0.001$, $Gr/Re = 100$, Kr = 652): **a** $r_q = 1$ and **b** $r_q = 0$

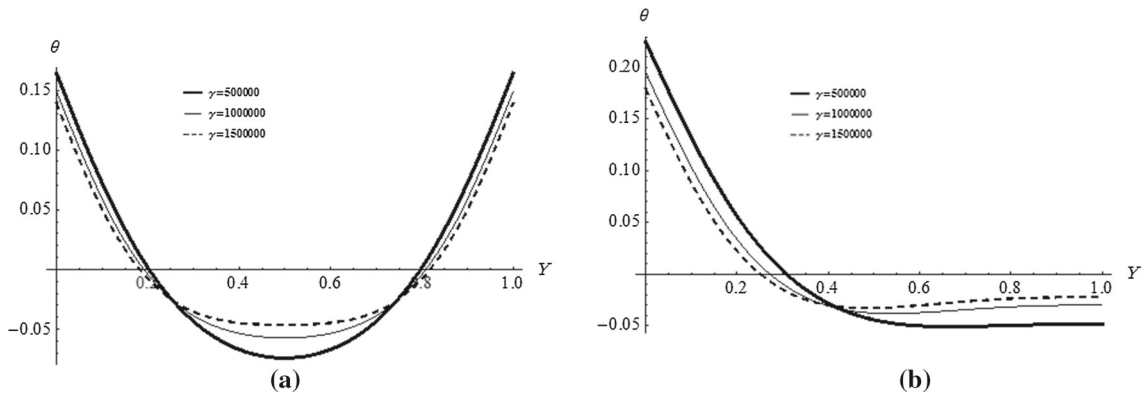

Fig. 9 Dimensionless temperature distribution of nanofluid for different values of γ ($\phi_0 = 0.001$, $Gr/Re = 100$, Kr = 652): **a** $r_q = 1$ and **b** $r_q = 0$

for two different types of nanoparticle materials (SiO_2 and Cu) at different values of volume fraction by using Eq. (24) to calculate Nu_{nf} and Nu_{bf} (i.e., when $\phi_0 \approx 0$) and then applying the following relationship:

$$\frac{h_{nf}}{h_{bf}} = \frac{Nu_{nf}}{Nu_{bf}} k_r \tag{26}$$

Table 2 compares the results with the correlation of Xuan and Roetzel [29] [Eq. (25)]. The comparison shows an excellent agreement between the two solutions with a maximum deviation of 0.066%.

In addition, the current solution for the velocity field in the absence of suspended nanoparticles ($\phi_0 = 0$) is identical to the solution given obtained previously [30] for the same parameter values. Additionally, the temperature distribution

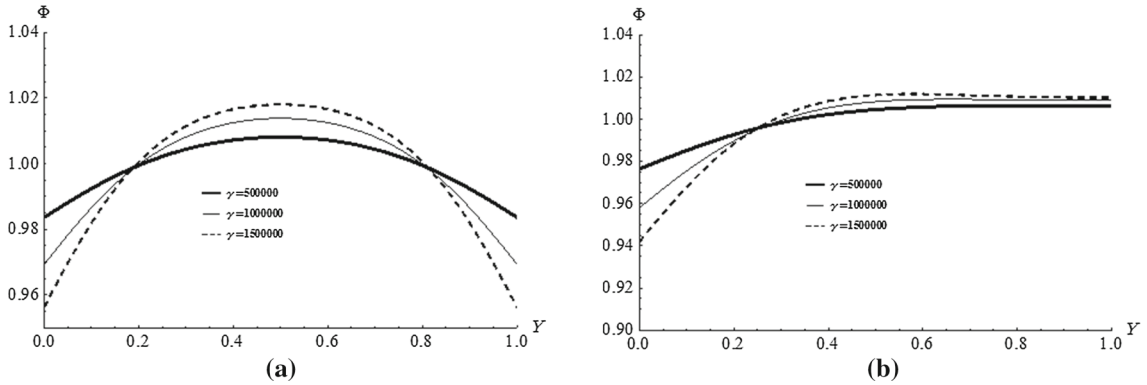

Fig. 10 Dimensionless particle distribution of nanofluid for different values of γ ($\phi_0 = 0.001$, $Gr/Re = 100$, Kr = 652): **a** $r_q = 1$ and **b** $r_q = 0$

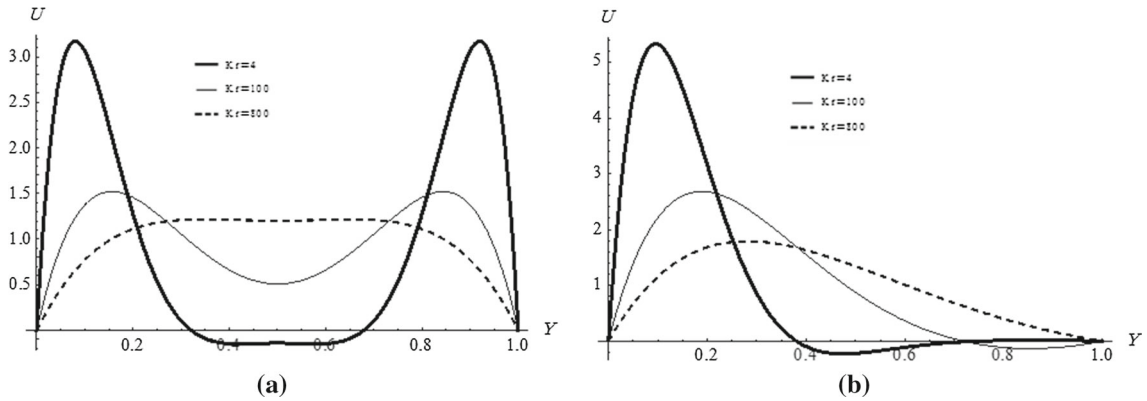

Fig. 11 Dimensionless velocity distribution of nanofluid for different values of Kr ($\phi_0 = 0.001$, $Gr/Re = 100$, $\gamma = 1{,}120{,}000$): **a** $r_q = 1$ and **b** $r_q = 0$

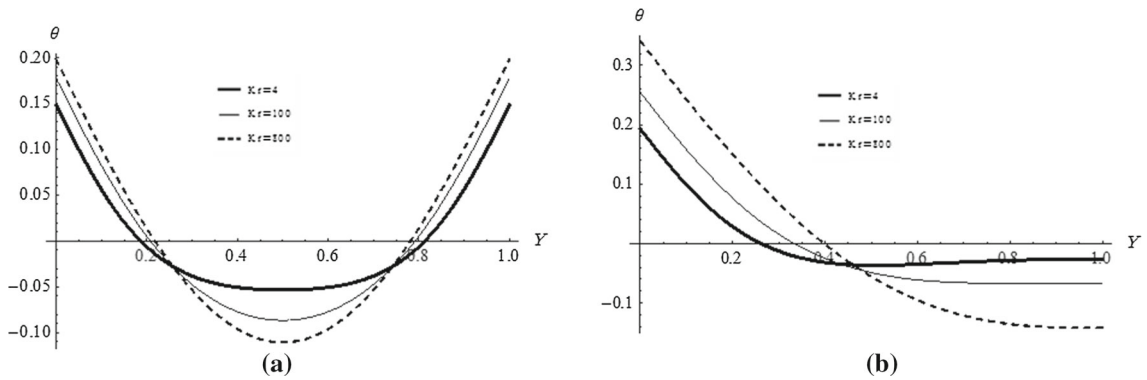

Fig. 12 Dimensionless temperature distribution of nanofluid for different values of Kr ($\phi_0 = 0.001$, $Gr/Re = 100$, $\gamma = 1{,}120{,}000$): **a** $r_q = 1$ and **b** $r_q = 0$

for the pure fluid case (i.e., $\phi_0 = 0$) exactly matches that presented previously [27]. Moreover, the closed-form analytical expressions presented in this paper for the velocity and its second derivative, pressure gradient, temperature and its second derivative, and nanoparticle distribution satisfy both the momentum and energy equations and the associated boundary conditions, and hence, the present analytical solutions are validated.

3 Results and Discussion

The addition of solid nanoparticles into the base fluid in the fully developed region produces three controlling parameters in addition to the well-known mixed-convection buoyancy parameter (Gr/Re) and the heat flux ratio ($r_q = q_2/q_1$). These three parameters are the immersed-particle buoyancy parameter (γ), nanoparticle volume fraction, and solid/fluid thermal conductivity ratio ($\mathrm{Kr} = K_p/K_{bf}$). The effect of

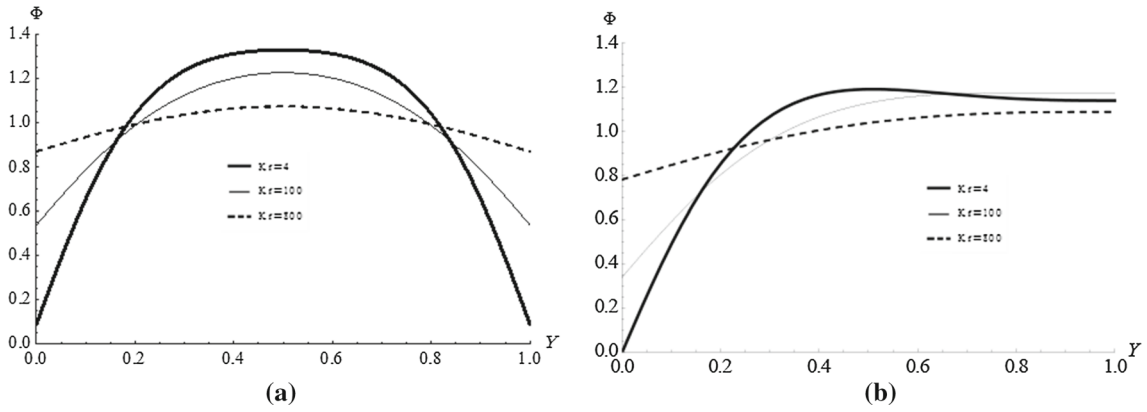

Fig. 13 Dimensionless particle distribution of nanofluid for different values of Kr ($\phi_0 = 0.001$, $Gr/Re = 100$, $\gamma = 1{,}120{,}000$): **a** $r_q = 1$ and **b** $r_q = 0$

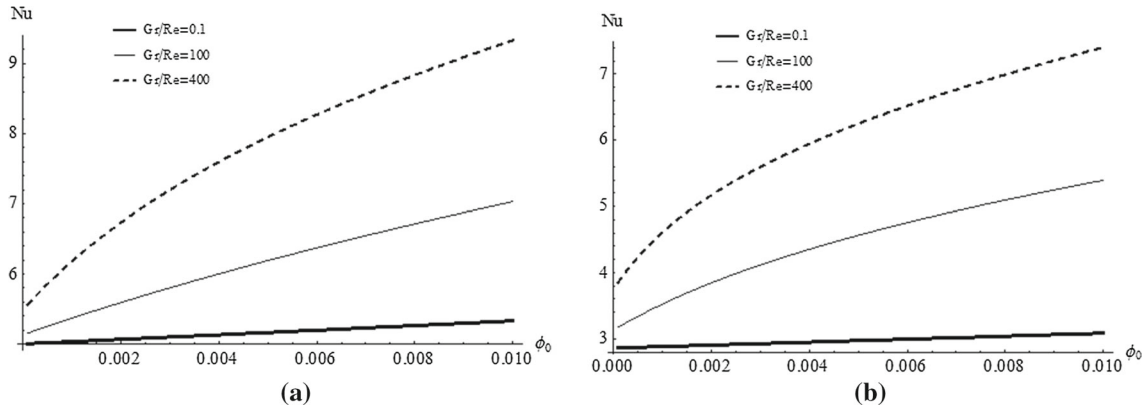

Fig. 14 Variations in local Nusselt number with ϕ_0 as a function of Gr/Re ($\gamma = 1{,}120{,}000$, Kr = 652): **a** $r_q = 1$ and **b** $r_q = 0$

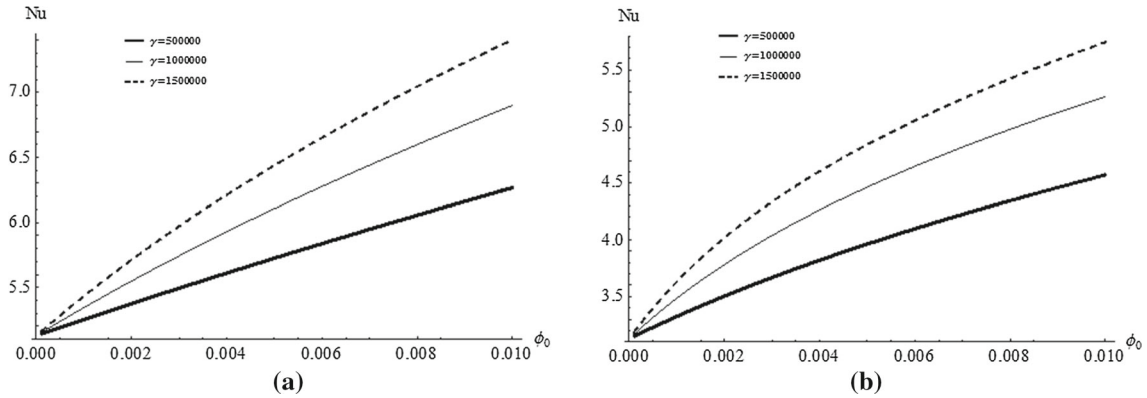

Fig. 15 Variations in local Nusselt number with ϕ_0 as a function of γ ($Gr/Re = 100$, Kr = 652): **a** $r_q = 1$ and **b** $r_q = 0$

these five parameters on the hydrodynamic and thermal performance is investigated and discussed.

Figure 2a, b shows the velocity distribution for three different values of the volume fraction during symmetric ($r_q = 1$) and asymmetric ($r_q = 0$) heating, respectively. It is clear from the figures that the axial velocity near the heated wall increases as the volume fraction increases. On the other hand, the velocity decreases in the core region of the channel during symmetric heating and near the unheated wall during asymmetric heating, which causes flow reversal. This effect is interpreted to be due to an increase in the immersed-particle buoyancy, which is caused by an increase in the volume fraction even when the mixed-convection buoyancy force decreases.

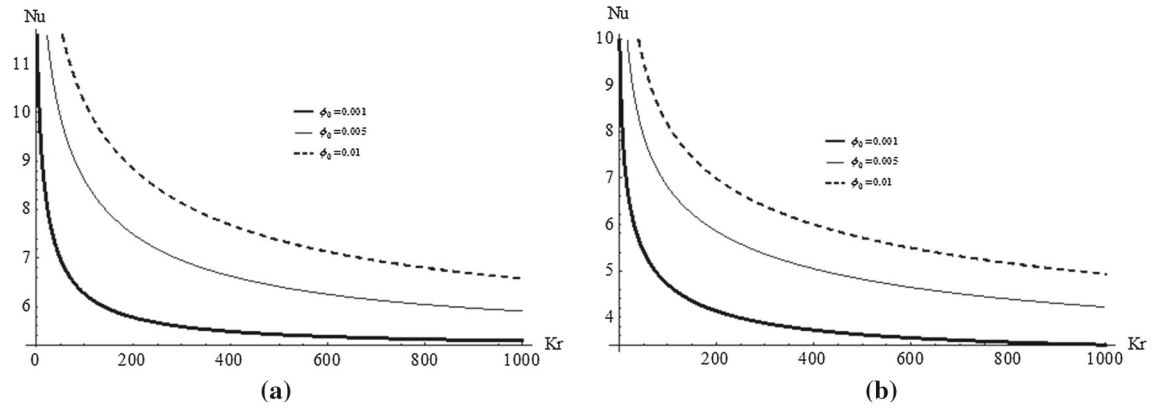

Fig. 16 Variations in local Nusselt number with Kr as a function of ϕ_0 ($Gr/Re = 100$, $\gamma = 1{,}120{,}000$): **a** $r_q = 1$ and **b** $r_q = 0$

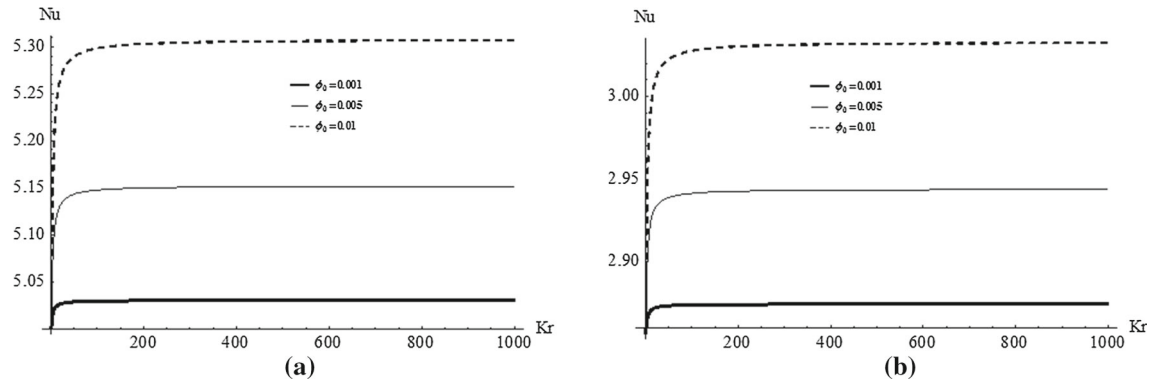

Fig. 17 Variations in local Nusselt number with Kr as a function of ϕ_0 ($Gr/Re = 0.001$, $\gamma = 1{,}120{,}000$): **a** $r_q = 1$ and **b** $r_q = 0$

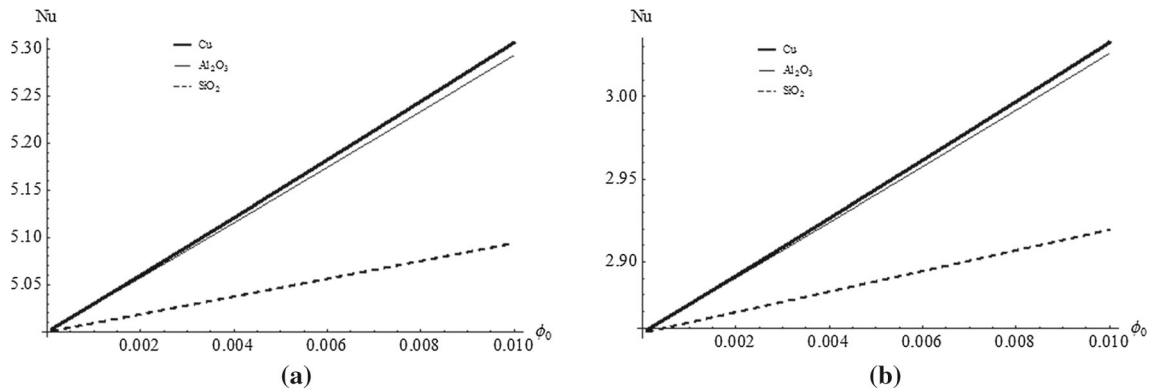

Fig. 18 Variations in local Nusselt number with ϕ_0 for three different kinds of nanoparticles ($Gr/Re = 0.001$, $\gamma = 1{,}120{,}000$): **a** $r_q = 1$ and **b** $r_q = 0$

In addition, an increase in the nanoparticle concentration in the base fluid increases the thermal conductivity of the nanofluid and hence enhances the heat transfer inside the channel. Therefore, the fluid temperatures near the heated wall decrease and those in the core region (during symmetric heating) or near the unheated wall (during asymmetric heating) increase, as shown in Fig. 3a, b (i.e., lower-temperature gradient inside the channel). Consequently, the thermophoresis force decreases, leading to particle migration from the high- to the low-particle-concentration region, as shown in Fig. 4a, b.

Figure 5a, b shows the effect of Gr/Re on the velocity profile during symmetric and asymmetric heating, respectively. The figures indicate an increase in the fluid velocities close to the heated wall and a decrease in the central channel during symmetric heating or close to the unheated wall during asymmetric heating, which, in turn, enhance the heat transfer rate at the heated wall because of momentum enrich-

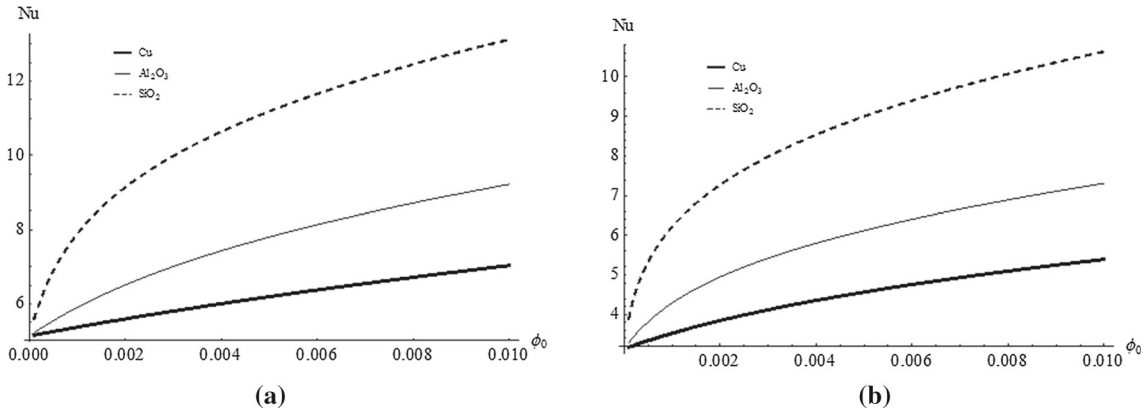

Fig. 19 Variations in local Nusselt number with ϕ_0 for three different kinds of nanoparticles ($Gr/Re = 100$, $\gamma = 1{,}120{,}000$): **a** $r_q = 1$ and **b** $r_q = 0$

ment, as shown in Fig. 6a, b. In addition, the thermophoresis force increases as Gr/Re increases because of a decrease in the fluid density. This, in turn, leads to nanoparticle depletion close to the heated wall and nanoparticle accumulation at the channel core during symmetric heating and close to the cold wall during asymmetric heating, as shown in Fig. 7a, b, respectively.

When nanoparticles are suspended in the fluid, the immersed-particle buoyancy parameter (γ) appears, which parameterizes the fluid motion due to solid/fluid density differences. When γ increases, the relative velocity between the solid nanoparticles and base fluid increases, leading to momentum productivity. Hence, the effects of γ on the velocity and temperature profiles are similar to those of the mixed-convection buoyancy parameter, as shown in Fig. 8a, b (velocity profile) and Fig. 9a, b (temperature profile). Increasing γ (by increasing either ρ_p or d_p) decreases the Brownian diffusion, resulting in particle migration that is controlled by the thermophoresis force, as shown in Fig. 10a, b.

Another factor investigated in the present problem is the solid/fluid thermal conductivity ratio (Kr). Its effects on the velocity, temperature, and particle concentration profiles are shown in Figs. 11, 12, and 13, respectively. On the one hand, conduction heat transfer increases as Kr increases. On the other hand, as Kr increases, the thermophoresis force acting on the nanoparticles immersed in the base fluid decreases and the immersed-particle buoyancy effect decreases, as shown in Fig. 11a, b. The reduction in the immersed-particle buoyancy effect decreases the heat transfer rate inside the channel, as shown in Fig. 12a, b. The nanoparticles eject themselves from the heated region toward the channel core during symmetric heating (Fig. 13a) or toward the cold plate during asymmetric heating (Fig. 13b) for low values of Kr. As Kr increases, the thermophoresis force decreases and the particle concentration tends to be uniform inside the channel, as shown in Fig. 13a, b. Given these observations, when the forced-convection flow is dominant ($Gr/Re < 1$), the use of high-thermal-conductivity nanoparticle solids is preferred to enhance conduction heat transfer. In contrast, low-thermal-conductivity particles are desirable for mixed-convection flow to enhance buoyancy.

The local Nusselt number on the heated wall is shown as a function of ϕ_o for three selected values of Gr/Re in Fig. 14 and for three selected values of γ in Fig. 15. As expected from the effects of these parameters on the hydrodynamic and heat transfer behavior explained earlier, Nu increases remarkably with Ge/Re, γ, and ϕ_o. The effects of Kr on the local Nusselt number are shown in Figs. 16 and 17 for mixed-convection (i.e., $Gr/Re > 1$) and forced-convection (i.e., $Gr/Re < 1$) flows, respectively. Nu decreases sharply and then gradually as Kr increases for mixed-convection flow. However, when forced convection is dominant, as Kr increases, Nu increases sharply and then gradually until it reaches an asymptotic value at Kr $\approx$ 50, as shown in the two figures. In addition, the figures indicate that the heat transfer performance is affected considerably by Kr variations at low and moderate values. However, its variation effects are negligible for forced-convection flow for Kr $\geq$ 50 and have relatively small significance for mixed-convection flow at high values of Kr (Kr $\geq$ 600). This result confirms the aforementioned conclusion that for better thermal performance, high-thermal-conductivity nanoparticles are preferred when the flow is driven solely by forced convection, whereas low-thermal-conductivity nanoparticles are desirable when the flow is driven by combined forced and natural convection. To test this result in practical materials, the variation in Nu with the volume fraction is analyzed for three selected nanoparticle materials—Cu, Al_2O_3, and SiO_2—for forced-convection flow (Fig. 18, $Gr/Re = 0.01$) and mixed-convection flow (Fig. 19, $Gr/Re = 100$). Cu, which has the highest thermal conductivity, has the highest Nu for forced-convection flow,

whereas SiO_2, which has the lowest thermal conductivity, has the highest Nu in the mixed-convection mode.

4 Conclusion

In this study, the mixed-convection flow of nanofluids between two asymmetrically heated vertical parallel plates in the fully developed region is considered. The momentum, energy, and nanoparticle concentration equations of the Buongiorno model are analytically solved. The solution is limited to tiny nanoparticles (diameter < 100 nm), for which the Brownian motion and thermophoresis force are significant. Closed-form formulas are deduced for the nanofluid velocity, temperature, and nanoparticle profiles as well as for the pressure gradient and Nu. The solution is strongly affected by the mixed-convection buoyancy parameter, immersed-particle buoyancy parameter, volume fraction, solid/fluid conductivity ratio, and heat flux ratio.

In particular, the results reveal the following:

- Nu significantly increases (up to 100%) with increasing volume fraction in the mixed-convection dominant regime and slightly increases (less than 10%) in the forced-convection dominant regime.
- In the mixed-convection dominant regime, Nu significantly decreases with increasing solid/fluid thermal conductivity ratio, and the reduction could be more than 60% at high values of Gr/Re.
- In the forced-convection dominant regime, Nu nonsignificantly increases with increasing solid/fluid thermal conductivity ratio and reaches its asymptotic value at $\mathrm{Kr} = 50$.

In view of the above remarks, the suspension of high-thermal-conductivity nanoparticle materials into the base fluid is useful when the flow is driven solely by forced convection. In contrast, low-thermal-conductivity nanoparticle materials are beneficial for improving heat transfer performance in the mixed-convection regime. These results are important for designing effective heat exchange systems in many engineering applications. For example, for nuclear applications, selecting copper nanoparticles is more useful to enhance the heat transfer in a forced-convection loop of a nuclear reactor. For cooling high-power electronic devices, where the buoyancy is comparable to the inertia force, SiO_2 nanoparticles are preferable. However, the thermophysical properties of nanofluids are strongly dependent on the nonuniform nanoparticle concentration in the channel. Hence, further study should be conducted to analyze the coupling of the nanoparticle concentration equation with the conservation equations of mass, momentum, and thermal energy.

References

1. Choi, S.U.S.: Enhancing thermal conductivity of fluids with nanoparticles. ASME Fluids Eng. Div. **231**, 99105 (1995)
2. Farbod, M.; Ahangarpour, A.; Etemad, S.G.: Stability and thermal conductivity of water-based carbon nanotube nanofluids. Particuology **22**, 59–65 (2015)
3. Hwang, K.S.; Jang, S.P.; Choi, S.U.S.: Flow and convective heat transfer characteristics of water-based Al_2O_3 nanofluids in fully developed laminar flow regime. Int. J. Heat Mass Transf. **52**(1–2), 193–199 (2009)
4. Hu, Z.S.; Dong, J.X.: Study on antiwear and reducing friction additive of nanometer titanium oxide. Wear **216**(1), 92–96 (1998)
5. Li, W.; Nakayama, A.: Temperature dependency of thermophysical properties in convective heat transfer enhancement in nanofluids. J. Thermophys. Heat Transf. **29**(3), 504–512 (2015)
6. Xing, M.; Yu, J.; Wang, R.: Experimental study on the thermal conductivity enhancement of water based nanofluids using different types of carbon nanotubes. Int. J. Heat Mass Transf. **88**, 609–616 (2015)
7. Nayak, R.K.; Bhattacharyya, S.; Pop, I.: Numerical study on mixed convection and entropy generation of a nanofluid in a lid-driven square enclosure. J. Heat Transf. **138**(1), 012503 (2015)
8. Hwang, K.S.; Jang, S.P.; Choi, S.U.S.: Flow and convective heat transfer characteristics of water-based Al_2O_3 nanofluids in fully developed laminar flow regime. Int. J. Heat Mass Transf. **52**(1–2), 193–199 (2009)
9. Maïga, S.E.B.; Nguyen, C.T.; Galanis, N.; Roy, G.: Heat transfer behaviors of nanofluids in a uniformly heated tube. Superlattices Microstruct. **35**(3–6), 543–557 (2004)
10. Mokmeli, A.; Saffar-Avval, M.: Prediction of nanofluid convective heat transfer using the dispersion model. Int. J. Therm. Sci. **49**(3), 471–478 (2010)
11. Serna, J.: Heat and mass transfer mechanisms in nanofluids boundary layers. Int. J. Heat Mass Transf. **92**, 173–183 (2016)
12. Buongiorno, J.: Convective transport in nanofluids. J. Heat Transf. **128**(3), 240–250 (2005). https://doi.org/10.1115/1.215083
13. Chen, C.-K.; Chen, B.-S.; Liu, C.-C.: Heat transfer and entropy generation in fully-developed mixed convection nanofluid flow in vertical channel. Int. J. Heat Mass Transf. **79**, 750–758 (2014)
14. Heris, S.Z.; Esfahany, M.N.; Etemad, G.: Numerical investigation of nanofluid laminar convective heat transfer through a circular tube. Numer. Heat Transf. Part A Appl. Int. J. Comput. Methodol. **52**(11), 1043–1058 (2007)
15. You, X.-C.; Xu, H.; Pop, I.: Analysis of fully developed opposing mixed convection flow in an inclined channel filled by a nanofluid. J. Heat Transf. **136**(12), 124502 (2014)
16. Xu, H.; Pop, I.: Fully developed mixed convection flow in a vertical channel filled with nanofluids. Int. Commun. Heat Mass Transf. **39**(8), 1086–1092 (2012)
17. Grosan, T.; Pop, I.: Fully developed mixed convection in a vertical channel filled by a nanofluid. J. Heat Transf. **134**(8), 082501 (2012)
18. di Schio, E.R.; Celli, M.; Barletta, A.: Effects of Brownian diffusion and thermophoresis on the laminar forced convection of a nanofluid in a channel. J. Heat Transf. **136**(2), 022401 (2014)
19. Elcock, D.: Potential impacts of nanotechnology on energy transmission applications and needs. Environmental Science Division, Argonne National Laboratory, United States, ANL/EVS/TM/08-3 (2007)
20. Yu, W.; France, D.M.; Choi, S.U.S.; Routbort, J.L.: Review and assessment of nanofluid technology for transportation and other applications. Argonne National Laboratory, United States, ANL/ESD/07-9, 10.2172/919327 (2007)

21. Al-Amri, F.; Mallick, T.K.: Alleviating operating temperature of concentration solar cell by air active cooling and surface radiation. Appl. Therm. Eng. **59**, 348–354 (2013)
22. Escher, W.; Brunschwler, T.; Shalkevich, N.; Shalkevish, A.; Burgi, T.; Michel, B.; Poulikakos, D.: On the cooling of electronics with nanofluids. J. Heat Transf. **133**, 051401 (2011)
23. Turkyilmazoglu, M.: Anomalous heat transfer enhancement by slip due to nanofluids in circular concentric pipes. Int. J. Heat Mass Transf. **85**, 609–614 (2015)
24. Mahdavi, M.; Sharifpur, M.; Meyer, J.P.: CFD modelling of heat transfer and pressure drops for nanofluids through vertical tubes in laminar flow by Lagrangian and Eulerian approaches. Int. J. Heat Mass Transf. **88**, 803–813 (2015)
25. Mital, M.: Semi-analytical investigation of electronics cooling using developing nanofluid flow in rectangular microchannels. Appl. Therm. Eng. **52**, 321e327 (2013)
26. Cimpean, D.S.; Pop, I.: Fully developed mixed convection flow of a nanofluid through an inclined channel filled with a porous medium. Int. J. Heat Mass Transf. **55**, 907–914 (2012)
27. Barletta, A.; Zanchini, E.: On the choice of the reference temperature for fully-developed mixed convection in a vertical channel. Int. J. Heat Mass Transf. **42**(16), 3169–3181 (1999)
28. Yang, C.; Li, W.; Sano, Y.; Mochizuki, M.; Nakayama, A.: On the anomalous convective heat transfer enhancement in nanofluids: a theoretical answer to the nanofluids controversy. J. Heat Transf. **135**(5), 054504 (2013). https://doi.org/10.1115/1.4023539
29. Xuan, Y.; Roetzel, W.: Conceptions for heat transfer correlation of nanofluids. Int. J. Heat Mass Transf. **43**, 3701–3707 (2000)
30. Avci, M.; Aydin, O.: Mixed convection in a vertical parallel plate microchannel with asymmetric wall heat fluxes. J. Heat Transf. **129**(8), 1091–1095 (2007)